First-principles calculations on the local magnetic properties of BCC Fe-Cr alloys

1991 J. Phys.: Condens. Matter 3 9141

(http://iopscience.iop.org/0953-8984/3/46/015)

J. Phys.: Condens. Matter 3 (1991) 9141–9149. Printed in the UK

First-principles calculations on the local magnetic properties of BCC Fe–Cr alloys

Zhiqiang Li†‡ and Helie Luo†

† Institute of Physics, Academia Sinica, Beijing 100080, People's Republic of China

‡ CCAST (World Laboratory), PO Box 8730, Beijing 100080, People's Republic of China

Received 15 May 1991, in final form 1 July 1991

Abstract. The embedded-cluster model within the framework of the discrete variational method is used to carry out self-consistent-field electronic structure calculations for the local magnetic moment, isomer shift and the hyperfine fields on several distinct iron sites in a disordered Fe–Cr alloy. We present these quantities as a function of the number of nearest and next-nearest Cr neighbours. Our results for the variations in these quantities due to the presence of Cr atom neighbours are in good agreement with experiment. The results are compared with the calculations on Fe–Si alloys.

1. Introduction

The magnetic properties of BCC Fe–Cr disordered alloys have been studied extensively for many years. Experiments showed that the $Fe_{1-x}Cr_x$ solid solution is ferromagnetic in the range of $x \leqslant 0.7$ and the spontaneous magnetic moment of such a solution disappears near $x = 0.8$ [1, 2]. After the collapse of ferromagnetism, mictomagnetic characters are observed and, in the Fe dilute region, antiferromagnetism and a SDW state are attained [3].

Recent studies of the magnetism of transition-metal alloys have revealed that the magnetic moments of metal atoms depend on their local environment rather than on their average electronic properties. Shiga and Nakamura [4] have studied the effect of local environment on the magnetic moment of BCC Fe–Cr alloys by Mössbauer spectra and discussed the hyperfine field distribution and magnetic properties by local model. Dubiel [5] and Dubiel and Zinn [6] have also investigated the charge and spin densities of disordered Fe–Cr alloys by the Mössbauer effect and found the relations of the hyperfine field and isomer shift with the numbers of Cr atoms at the first- and second-neighbour shells.

Compared with a large number of experimental investigations, there have been few theoretical studies on the local magnetic properties of disordered Fe–Cr alloys. Hasegawa and Kanamori [7] have studied the electronic and magnetic structure of Fe–Cr by the coherent-potential approximation (CPA); the results include the density of states and the magnetic moment as a function of Cr concentration. Recently, Ebert *et al* [8] have also calculated the hyperfine fields of the substitutional disordered BCC Fe_xCr_{1-x} alloy by the KKR CPA method. However, the CPA emphasizes, on the average,

0953-8984/91/469141 + 09 $03.50

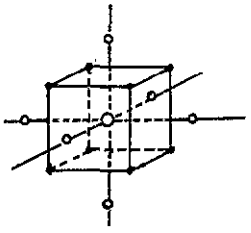

Figure 1. The geometry of the Fe_{15} cluster for BCC iron: ○, central site; ●, nearest neighbour; ◇, *next-nearest neighbour*.

magnetic properties as a function of Cr concentration and neglects the local environment effects.

The *self-consistent field* (SCF) *molecular orbital* (MO) *discrete variational method* (DVM) [9] has been proved to be a powerful technique for studying the local effects by a small cluster with a desired atom configuration. We have studied the local magnetic moment and hyperfine interactions of disordered Fe–Si alloys using this method [10] and obtained satisfactory results compared with experiments. As an extension, we performed the first-principles calculation on the electronic and magnetic structure of Fe–Cr alloys by the spin-polarized embedding scheme, hoping to give a theoretical description of the experimental results. The basic question that we want to answer is how the magnetic moment, spin and charge density vary with the number of Cr atoms at neighbouring shells.

In treating disordered or impurity magnetic properties of transition metals, where the local order may be a dominant factor rather than the long-range periodicity because these properties are chiefly determined by the quasilocalized d electrons, representation of the system by a small embedded cluster is not only computationally attractive but also physically reasonable.

2. Theoretical approach

Clusters with 15 atoms, as depicted in figure 1, were considered to represent the undistorted BCC iron matrix; it consists of eight nearest neighbours (NNS) and six next-nearest neighbours (NNNS). The influences of Cr atoms were studied by substitution of one to eight NN Fe atoms and four to six NNN Fe atoms, which are used as representations of disordered Fe–Cr alloys. In all cases the cluster was embedded in the Fe–Cr crystal which are the periodic translation of the corresponding cluster. For convenience, we use the nomenclature C(N, M) to represent the cluster having N NN Cr atoms and M NNN Cr atoms.

The electronic structure of the clusters were calculated with the first-principles DVM within the local density functional theory [11]. The same method was employed in several other calculations on metal clusters [9, 10, 12] and has been described in detail previously [13].

The spin-polarized one-electron equations

$$(h_\sigma - \varepsilon_{j\sigma})\phi_{j\sigma}(r) = 0 \tag{1}$$

are solved self-consistently, where the wavefunctions $\phi_{j\sigma}(r)$ for different spins σ are

allowed to have different spatial extensions. The one-electron Hamiltonian, in atomic units, is

$$h_\sigma = -\tfrac{1}{2}\nabla^2 + V_{\mathrm{Coul}}(\rho_\sigma) + V_{\mathrm{xc}}(\rho_\sigma). \tag{2}$$

The electronic density at point r is a sum over the spin-dependent MOS $\phi_{j\sigma}$ with occupation $n_{j\sigma}$:

$$\rho_\sigma(r) = \sum_j n_{j\sigma} |\phi_{j\sigma}(r)|^2. \tag{3}$$

$V_{\mathrm{xc}}(\rho_\sigma)$ was chosen to be of the spin-polarized von Barth–Hedin [14] form.

In the DVM the MOS are expanded on a basis of numerical atomic orbitals (LCAO). Sphere potential wells around the atoms are employed to obtain more contracted valence orbitals, these include 3s, 3p, 3d, 4s and 4p for central Fe and 3d, 4s and 4p for other Fe and Cr. Other low-lying orbitals are kept frozen in all cases. The secular equation $(\mathbf{H} - E\mathbf{S})\mathbf{C} = 0$ are solved self-consistently using matrix elements determined by numerical integrations on a three-dimensional grid. In the usual DVM, a random integration method (diophantine) [13] is employed; however, in the case of hyperfine interactions, the calculations require much greater caution in the numerical procedures, especially at the core region of the probe atom, where the precision of matrix elements for the rapidly varying functions is difficult to achieve. Thus a special integration scheme in spherical volumes about a particular atom was developed [15]. In the present work, we are primarily interested in the hyperfine fields of the central Fe atom and have replaced the diophantine points in the core region by a dense regular (angular × radial Gaussian quadrature) mesh.

In the self-consistent-charge (SCC) approximation, the actual electronic density is replaced by a model density $\rho_\sigma^{\mathrm{scc}}(r)$, which is a superposition of radial densities R_{nl}^v centred on cluster atoms via the diagonal-weighted Mulliken population f_{nl}^v:

$$\rho_\sigma^{\mathrm{scc}}(r) = \sum_{nl} \sum_v f_{nl}^v |R_{nl}(r_v)|^2. \tag{4}$$

Finally, an embedding scheme [13] is employed to simulate the effect of the rest of the microcrystal on the cluster. It consists basically of placing numerical atomic potentials at about 300 closest sites surrounding the cluster. In order to make the comparison reliable, all the input parameters remained unchanged, such as the atomic basis functions, integration points and crystal potentials.

The isomer shift (IS) of an absorber A relative to a source S in a Mössbauer nuclear γ-resonance measurement is given by (see, e.g., [16])

$$\mathrm{IS} = \alpha[\rho_{\mathrm{A}}(0) - \rho_{\mathrm{S}}(0)]. \tag{5}$$

α is called the IS calibration constant. For ^{57}Fe, the reported values of α vary from -0.11 to $-0.51 a_0^3$ mm s^{-1}, where a_0 is the Bohr radius. We took $\alpha = -0.25 a_0^3$ mm s^{-1} which is close to a recent estimate [12]. We have neglected 1s and 2s contributions since the computed difference in $\rho(0)$ for these orbitals in different environments is negligible [15].

The hyperfine magnetic field seen by probe nucleus is given by [17]

$$H_{\mathrm{c}} = \tfrac{8}{3}\pi g \mu_{\mathrm{B}} (\langle S \rangle / P)[\rho_\uparrow(0) - \rho_\downarrow(0)] = B\,\Delta\rho(0)\ \mathrm{kG} \tag{6}$$

where S is the total spin of ion with P unpaired electrons, g is the electronic g-factor and μ_{B} is the Bohr magneton. $\rho_\uparrow(0) - \rho_\downarrow(0)$ is the s spin density at the nucleus which was

Table 1. Local magnetic moment of the central site in cluster. $C(N,M)$ indicates a cluster with N and M Cr atoms at NN and NNN shells.

Cluster	$C(0,0)$	$C(1,0)$	$C(2,0)$	$C(4,0)$	$C(8,0)$	$C(0,4)$	$C(0,6)$
Symmetry	O_h	C_3	D_{3d}	T_d	O_h	D_{4h}	O_h
Central Fe							
μ_{3d} (μ_B)	3.18	3.01	2.66	2.49	1.68	3.07	2.80
μ_{4s+4p}	−0.39	0.02	0.07	0.08	0.18	−0.11	−0.11

calculated respectively for spin up and spin down, and B is a constant and equal to $524.2(e/a_0^3)^{-1}$ kG.

3. Results and discussion

3.1. Magnetic moment

For a cluster with inequivalent sets of atoms in different environment, it is natural that the central atom with its coordination shells complete may best describe the properties of corresponding bulk solid. This is confirmed by many calculations on metallic clusters [15, 18] and in accord with intuition.

We have used several distinct clusters to study the local magnetic moment at Fe sites and its changes as Cr atom substituting the Fe atom at NN and NNN shells. In table 1, we present the 3d and 4s+4p magnetic moments at the central site, which were calculated by taking the difference of the spin-up and spin-down Mulliken populations [19]. Note that the recalculated results for the $C(0,0)$ cluster are very similar to those in [10]. There are various locations of Cr atoms in the cluster $C(2,0)$ or $C(4,0)$; we considered only the most probable configuration, in Fe-rich alloy, with higher symmetry.

We find that, for the pure iron cluster $C(0,0)$, the total magnetic moment at the central site of 2.79 μ_B is quite larger than the experimental value of 2.2 μ_B. As noted before for other magnetic materials [15, 18], this is a finite cluster effect because the overlap of orbital wavefunctions in the cluster is not so complete as that in the bulk solid. However, the central Fe is the most bulk-like atom and, as we take more atom shells into account, the cluster size effect can be reduced. Many calculations have indicated that, for most physical properties, the three- to four-atomic-shell cluster is sufficient [9, 12, 15].

It is noted that the 3d moment of the central site decreases with increasing Cr substitutions in the NN shell, but the total magnetic moment increases a little when there is one Cr atom in the first-neighbour shell (figure 2). Hamada [20] has indicated that the magnetic moment of an atom in a transition-metal alloy is primarily determined by its NN environment. In this simple form, Shiga and Nakamura [4] have given the Fe atom moment as a function only of its number of Cr atoms at the NN shell, which is shown in figure 2. The calculated values have the same variance trend as experiment, indicating that the DVM is capable of calculating the relative changes more accurately. From table 1, we note that, when the Cr atoms are located in the NNN shell, their influences on the magnetic moment of central Fe are much smaller than that when the Cr atoms are in the NN shell. For comparison, the results of Fe–Si alloys are also shown in figure 2.

From table 1, we note that the 4s + 4p magnetic moment is negative in the pure Fe cluster $C(0,0)$ and becomes positive when there are Cr atoms in the cluster. The magnetic

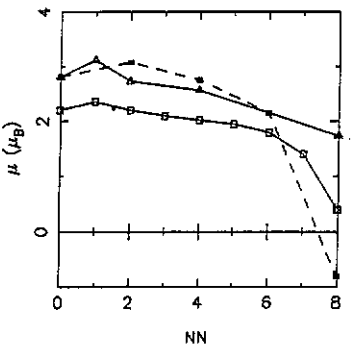

Figure 2. Magnetic moment of Fe atom as a function of NN Cr atoms: △, calculated; □, experiment [4]; ■, corresponding values for Fe–Si alloys [10]

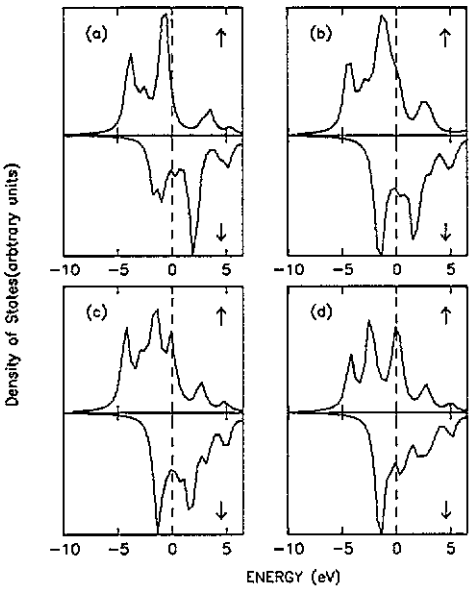

Figure 3. 3d DOS of central Fe in (*a*) *C*(0,0), (*b*) *C*(2,0), (*c*) *C*(4,0) and (*d*) *C*(8,0) clusters. The spin-up and spin-down bands are normalized to the same scale within each cluster.

moments of these valence bands are induced by hybridization of the orbitals of the valence and 3d bands, which have been found experimentally to be negative [21] in BCC iron and is sensitive to the environment. Since the s and p electrons interact antiferromagnetically with the neighbouring d electrons, as pointed out by Anderson and Clogsten [21], thus the s–d and p–d interactions lead to negative 4s and 4p moments. With the appearance of Cr atoms in the first and second shells and because the Cr 3d moment is negative (see below), the 4s and 4p moment start to change direction from negative for a pure Fe cluster *C*(0,0) to positive for a *C*(2,0) cluster and increase steadily as *N* increases. Thus the Cr atoms decrease the Fe 3d moment and increase the 4s + 4p moment, which gives the maximum of the total magnetic moment curve in figure 2.

In most cases we find the Cr 3d moment to be about $-(3.3\text{–}3.4)\ \mu_B$ antiferromagnetically coupled with Fe atoms, which are comparable with the calculation of Fe–V interfaces in [22].

3.2. Density of states

The energy spectrum of valence eigenfunctions is best displayed as a density of states (DOS). The contribution of state *nl* of atom *v* to the DOS is represented by

$$D^v_{nl}(E) = \sum_p f^v_{nl,p} \frac{\sigma/\pi}{(E-\varepsilon_p)^2+\sigma^2} \tag{7}$$

where $f^v_{nl,p}$ is the Mulliken population contribution to the *p*th MO. The Lorentzian width parameter σ was chosen to be 0.1 eV. The total DOS in the DVO MO method consists of the contributions from all the atoms in the cluster and is not so accurate and instructive

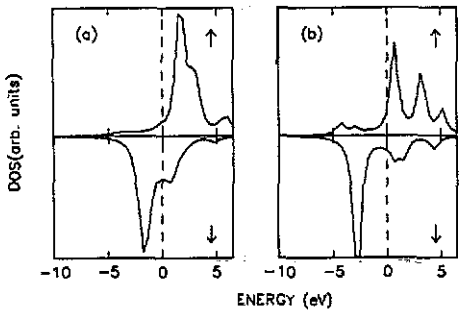

Figure 4. (*a*) Cr 3d DOS of $C(1,0)$ cluster; (*b*) Cr 3d DOS of $CrFe_{14}$ cluster.

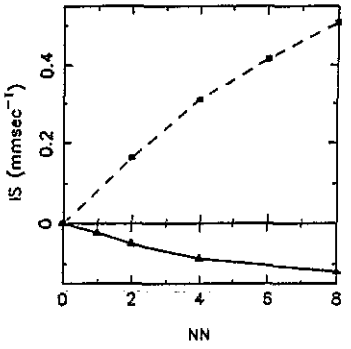

Figure 5. ISS of Fe atom as a function of NN Cr atoms (△) and as a function of NN Si atoms [10] (■).

as the partial DOS of the central atom. Thus we depicted only the 3d DOS in figure 3. The 3d DOS of cluster $C(1,0)$ does not change considerably with $C(0,0)$; we did not plot it in figure 3.

From figure 3 we can see that the 3d DOS of $C(0,0)$ is quite similar to the DOS calculated from the band structure [23] although there is less fine structure because we do not include the 4s and 4p contributions. As the number of Cr atoms in the neighbouring shells increases the profile of the majority band of the central Fe 3d band is lowered (figure 3), while the minority band peak below E_F increases. This obvious change accounts for the 3d magnetic moment decrease.

We have studied a $CrFe_{14}$ cluster, where the central Fe atom in the Fe_{15} cluster was replaced by a Cr atom. The Cr 3d DOSs in the cluster $C(1,0)$ and in $CrFe_{14}$ are presented in figure 4. Figure 4(*b*) for dilute Cr in Fe is in good agreement with the KKR calculation [24]. We note that majority spin is near E_F while minority spin is below E_F, about -2.0 eV, concomitantly located with the 3d minority spin of Fe, which means the Cr d ↓ and Fe d ↓ electrons may have considerable interactions.

In our previous paper [10] we have ascribed the 3d magnetic moment reduction in disordered Fe–Si alloys to the p–d hybridizations. The situation in the Fe–Cr alloys is quite different. The interactions between Cr d ↓ and Fe d ↓ electrons may lower the potentials of the minority 3d band compared with the corresponding majority band; thus, the spin-up electrons transfer to the spin-down 3d band, resulting in the reduction in the 3d magnetic moment of Fe and making the 3d magnetic moment of Cr negative. This is also the reason for the lowering of the Fe 3d ↑ peak.

3.3. Isomer shift and hyperfine field

The IS is a measure of depletion or accumulation of the electronic charge at the probe nucleus. We have calculated the IS relative to pure iron according to equation (5) for $C(N,0)$ clusters and the results are depicted in figure 5. The calculation results of Fe–Si clusters are also shown in the same figure for comparison.

It is noted that the IS are positive values for Fe–Si alloys, while they are small negative values for Fe–Cr alloys, indicating that the charge transfer for these two alloys are opposite, from Fe to Si in Fe–Si alloys and from Cr to Fe in Fe–Cr alloys, in agreement with their electronegativity: Fe, 1.82; Si, 1.90; Cr, 1.66. Dubiel and Zinn [6] have found

Table 2. Hyperfine field of Fe–Cr clusters. N is the number of Cr atoms in the cluster. n_d and n_s are the Mulliken populations for the 3d and 4s orbitals respectively. H_f is the hyperfine field of core and valence electrons.

Cluster	n_d	n_s	H_f	ΔH_f (kG)	$\Delta H_f/N$	Experimental $\Delta H_f/N$[a]
$C(0,0)$	6.660	0.770	−422	—	—	
$C(1,0)$	6.655	0.772	−386	36	36	
$C(2,0)$	6.642	0.801	−346	76	38	31.9
$C(4,0)$	6.642	0.812	−320	102	26	
$C(8,0)$	6.634	0.835	−196	226	28	

$B = 524.2\ (e/a_0^3)^{-1}$ kG was used to calculate H_f.

[a] From [6].

that the isomer shift of Fe is on average $-0.020\ mm\ s^{-1}$ when there is one Cr atom in the first-neighbour shell of central Fe; our calculation is in good agreement with their Mössbauer studies.

The magnetic hyperfine field H_f of iron is often regarded as a measure of the magnetic moment on the Fe site. Conveniently, it can be decomposed into two contributions for transition metal [17]:

(i) a large negative contribution due to the exchange polarization of the core electron by d moment, referred to as the Fermi contact field;
(ii) the contribution from the valence electrons.

It was reported that the hyperfine field has a distribution in the Fe–Cr alloys [25]. Therefore, different local environments coexist in the Fe–Cr alloys. We have calculated the hyperfine field for six distinct local configurations representing the disordered Fe–Cr alloys using equation (6). The valence contribution can be obtained directly from our self-consistent MO calculation and includes all occupied wavefunctions belonging to the totally symmetric representation of the cluster point group. However, the core electron contribution requires greater caution because the hyperfine interaction involves a delicate balance of two large numbers for spin-up and spin-down density in the core region and, in the present cluster calculations, there is not enough variational freedom nor numerical precision to obtain the core spin density. We used the atomic configuration obtained by Mulliken analysis to perform atomic self-consistent calculations in the X_α approximation. This approach has been employed for many cases [12, 18].

The calculated H_f of pure BCC iron is 422 kG, which is somewhat larger than the experimental value of 339 kG. We should point out that, apart from the cluster size effect, both the atomic X_α treatment of the Fermi contact field and the relativistic effect can strongly affect the H_f value [18].

Dubiel and Zinn [6] have found that the hyperfine field reduction due to one Cr atom in the NN shell is -31.9 ± 0.8 kG. This value was found to be independent of the concentration of Cr, indicating that the localized character of spin density is dominantly determined by the neighbouring two atomic shells. We also calculated this difference in six different clusters using

$$\Delta H_f = H_f(\text{alloy}) - H_f(\text{iron}) \tag{8}$$

and list the results in table 2. We find that, on average, one Cr atom in the NN shell may

reduce H_f by about 26–34 kG, which is in very good agreement with experiment. It seems that the effects mentioned above which can affect the calculation of H_f(iron) and H_f(alloy) are partially cancelled when we calculate ΔH_f. This may be responsible for the observed good agreement between our results and experiment.

It is worth pointing out that H_f decreases with increasing number of Cr atoms in the NN shell but the total magnetic moment of central Fe does not show this trend; this can be attributed to the 4s + 4p moment which is negative in pure iron and becomes positive when there are Cr atoms in the cluster.

We now discuss the charge and spin-density distributions in detail. We note that the IS (negative) increases in magnitude and the hyperfine field (negative) decreases in magnitude as there are Cr atoms in the vicinity of central Fe atom; the former means that the charge density at the nucleus of central Fe site increases and the latter means the spin-down density decreases relative to spin-up density as the neighbouring Fe are replaced by Cr atoms.

From table 2, we find that the 4s Mulliken populations increase as N increases in the cluster $C(N,0)$, while the 3d Mulliken populations decrease. The former is consistent with their electronegativities and contributes to the increase in charge density at the central Fe nucleus. Watson and Bennett [26] have suggested that the 3d charge transfer in the transition metals and compounds is in opposite direction to that expected from their electronegativities. This is the case in our calculations; the 3d electrons of central Fe transfer to the neighbouring Cr atoms. The decrease in the number of 3d electrons leads to less shielding of the Fe nucleus and hence to a larger s electron density at the origin. In the Fe–Si alloys, we find that the IS is positive and increases as the number of Si atoms at the first-neighbour shell increases, while H_f is negative and decreases in magnitude. This indicates that the charge density at the nucleus of the probe atom decreases and so does the spin-down density. It should be pointed out that one must take care when using the IS to measure the charge transfer because the IS is determined only by s electrons.

4. Conclusions

We have calculated the electronic structure, local magnetic moment, IS and hyperfine interactions of Fe–Cr disordered alloys by the self-consistent spin-polarized embedding molecular cluster method and compared them with the available experiments. Our results show the following.

(i) The local moment of Fe is greatly influenced by the first-shell Cr atoms, but the effect is very small when the Cr atom is located in the second shell. The changes in d moment are ascribed mainly to the d $\downarrow$ − d $\downarrow$ overlaps in the Fe–Cr alloy.

(ii) The profile of the Fe d $\uparrow$ band is obviously reduced and the major peak of the Fe d $\downarrow$ band is greatly increased by the Cr atoms in the cluster.

(iii) The calculated IS are negative, which means that there is little charge transfer from neighbouring Cr atoms to the central Fe atom; this is in good agreement with experiment.

(iv) The hyperfine fields are found to be negative and decrease in magnitude with increasing number of Cr atoms in the neighbouring shells, which is consistent with experiment, indicating that the spin-down density is reduced relative to the spin-up density. H_f is not proportional to the total magnetic moment of Fe owing to the negative polarization of the 4s and 4p band.

From our studies, we conclude that, to calculate the properties of bulk by a cluster model, the cluster size may somewhat affect the absolute values of the calculated properties but the relative trend can be obtained quite accurately, which is usually more important in physical studies. Moreover, evidence [9] has been accumulated that, as the cluster size increases, the cluster model tends to the same limit as band-structure method and the 15 transition atom clusters that we used resembles a bulk solid well in many aspects.

Acknowledgments

This work was performed on the VAX8550 of CCAST, World Laboratory. LZQ is grateful to Ms Zeng Zhi for helpful discussions.

References

[1] Nevitt M V and Aldred A J 1963 *J. Appl. Phys.* **34** 463
[2] Ishikawa Y, Tournier R and Filippi J 1965 *J. Phys. Chem. Solids* **26** 1727
[3] Shull R D and Beck P A 1974 *AIP Conf. Proc.* **24** 95
[4] Shiga M and Nakamura N 1980 *J. Phys. Soc. Japan* **49** 528
[5] Dubiel S M 1976 *Acta Phys. Pol.* A **49** 619
[6] Dubiel S M and Zinn W 1981 *J. Magn. Magn. Mater.* **23** 214
[7] Hasegawa H and Kanamori J 1972 *J. Phys. Soc. Japan* **33** 1607
[8] Ebert H, Winter H, Johnson D D and Pinski F J 1990 *J. Phys.: Condens. Matter* **2** 443
[9] Press M R, Liu F, Khanna and Jena P 1988 *Phys. Rev.* B **40** 399
[10] Li Z Q, Luo H L, Lai W Y and Zheng Q Q 1991 *J. Phys. Condens. Matter* **3** 6649
[11] Kohn W and Sham L J 1965 *Phys. Rev.* **140** A 1133
[12] Elzain M E, Ellis D E and Guenzburger D 1986 *Phys. Rev.* B **34** 1430
[13] Ellis D E 1968 *Int. J. Quantum. Chem. Symp.* **35** 2
Ellis D E and Painter G P 1970 *Phys. Rev.* B **2** 2887
[14] von Barth U and Hedin L 1972 *J. Phys. C: Solid State Phys.* **5** 1629
[15] Guenzburger D and Ellis D E 1985 *Phys. Rev.* B **31** 93
[16] Greenwood N W and Gibb T C 1971 *Mössbauer Spectroscopy* (London: Chapman and Hall) p 386
[17] Watson R E and Freeman A J 1961 *Phys. Rev.* **123** 2027
[18] Chachan H, Galvao da Silva E, Guenzburger D and Ellis D E 1987 *Phys. Rev.* B **35** 1602
[19] Mulliken R S 1933 *Phys. Rev.* **45** 87
[20] Hamada N 1979 *J. Phys. Soc. Japan* **46** 1759
[21] Anderson P W and Clogsten A M 1961 *Bull. Am. Phys. Soc.* **6** 124
[22] Elzain M E, Ellis D E and Guenzburger D 1986 *Phys. Rev.* B **34** 1430
[23] Moruzzi V L, Janak J F and Williams A R *Calculated Electronic Properties of Metals* (Oxford: Pergamon)
[24] Drittler B, Stefanou N, Blügel S, Zeller R and Dederichs P H 1989 *Phys. Rev.* B **40** 8203
[25] Shiga M and Nakamura Y 1976 *Phys. Status Solidi* a **37** K89
[26] Watson R E and Bennett L H 1978 *Phys. Rev.* B **18** 6539